JOURNAL OF THERMOPHYSICS AND HEAT TRANSFER
Vol. 9, No. 3, July–September 1995

Visualization of Solidification Process in Kinetics Control System with Interferometry

Akira Iwasaki,* Shunsuke Hosokawa,† and Isao Kudo†
Electrotechnical Laboratory, Ibaraki 305, Japan
and
Hideo Takei,‡ Yoshito Arai,‡ Toru Watanabe,‡ and Takatoshi Kawai‡
Ishikawajima–Harima Heavy Industries, Tokyo 100, Japan

The behavior of a solid–liquid interface and temperature distribution in the supercooled melt during solidification were observed. Salol, an organic material, was solidified in a temperature gradient environment, where the process was controlled by both kinetics and diffusion. The thickness of the temperature-reversed layer in front of the interface was measured by interferometry with the moiré technique. It was found that as the interface advanced, the macroscopic roughness of the interface increased markedly in the flight experiment on a sounding rocket. Heat transfer during solidification was numerically calculated and was compared with experimental data.

Nomenclature

C_p = specific heat at constant pressure
D = diffusion coefficient
$f(T_i)$ = growth rate in the isothermal condition
L = latent heat
l = diffusion length
$R(t)$ = position of freezing point
T = temperature
t = time
$V(t)$ = growth rate, $dR(t)/dt$
Z = cell dimension
z = spatial coordinate
α = thermal diffusivity, $\lambda/\rho C_p$
η = independent variables defined by Eqs. (4) and (5)
λ = thermal conductivity
ρ = density

Subscripts
i = interface
l = liquid
s = solid

Introduction

THE buoyancy-free condition in microgravity is expected to be useful for the study of solidification processes such as the evolution of microstructure.[1] Investigation of the behavior of phase change materials is also important for thermal storage in space. Several attempts to elucidate the effect of microgravity on heat and mass transfer in the liquid, and the form of the interface have been reported in Refs. 2 and 3. An optical in situ observation technique has been applied to a transparent material, and can directly provide detailed information on the fundamental processes such as a growth form of the interface and a heat transfer. Interferometry can be used to obtain quantitative values on the distributions of temperature and concentration.

In a previous paper,[4] we developed a sophisticated Mach–Zehnder interferometer that could endure the launching environment. We visualized the interface during phase transition of a liquid crystal material, and showed that the microconvection on the ground deformed the interface. By contrast, the convection was suppressed in a microgravity environment and a faceted interface became larger. We have also observed a temperature-reversed layer in front of the interface in the supercooled melt, which was caused by the conduction of the released latent heat to the supercooled liquid; however, its thickness was not measured quantitatively.

In this study, we use salol, which grows with a faceted interface, and visualize the growth rate and the temperature distribution in the liquid adjacent to the interface. The method to simulate both the kinetics-controlled interface and the diffusion process of the latent heat in the melt is discussed. A microgravity experiment was conducted on the sounding rocket, MASER-5, using the same equipment as that in the previous study.

Experimental

The experimental setup was slightly modified to solve the problems encountered in the previous study[4]:

1) The Mach–Zehnder interferometer provided only infinite fringes, and the temperature on the interface was not accurately obtained.

2) The stiffness of the observation window of the experimental cell was not large enough to be free from distortion due to the compression force required to seal the sample. The inner dimensions were 13 mm (height) × 15 mm (width) × 2 mm (depth), and the thickness of the quartz glass window was 1 mm.

3) A liquid crystal material (5OCB) was used to observe two phase changes. However, the liquid crystal phase was not sufficiently transparent and the interferometric fringes were not clear.

4) Each grain of the sample was supercooled too much to permit observation with the optical system.

Figure 1 shows a Mach–Zehnder interferometer and typical interferograms for this experiment. The interferometer was modified by inserting an optical wedge plate with an angle of 20 deg into half of the reference beam, which made it possible to observe both infinite and finite fringes. The finite fringe method provided high spatial resolution of the temperature distribution (especially on the interface), where fringes with intervals of 0.2 mm were formed.[5] It was also useful to measure the thickness of the temperature-reversed layer in front

Received Dec. 27, 1993; revision received Nov. 25, 1994; accepted for publication Nov. 29, 1994.

*Researcher, Space Technology Section, Umezono, Tsukuba.
†Researcher, Space Technology Section, Umezono, Tsukuba. Member AIAA.
‡Researcher, Space Development Division, Otemachi, Chiyoda.

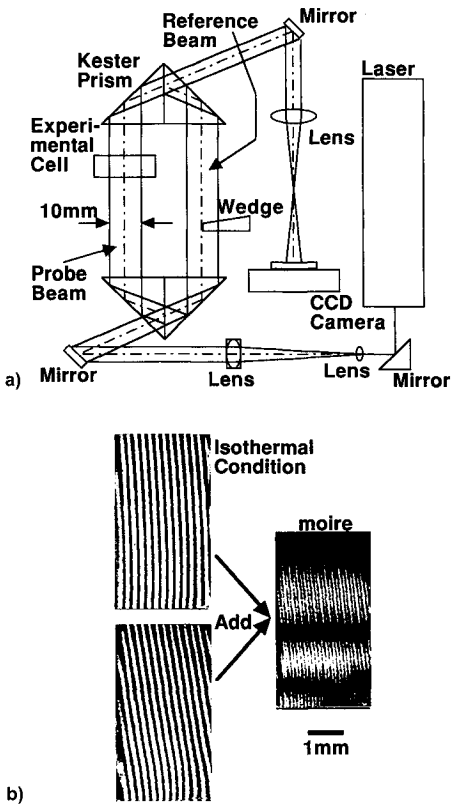

Fig. 1 Mach–Zehnder interferometer with moiré technique: a) interferometer and b) moiré technique.

of the interface by obtaining the maximum value of the refractive index. By contrast, the infinite fringe method was used in the remaining half to directly observe isothermal lines; this allowed better observation of the interface.

Space frequency of the finite fringes formed by the wedge was higher than that due to the temperature distribution, but lower than that of the resolution of a charge-coupled device (CCD) camera. Figure 1b shows an example of the moiré technique, in which two interferograms at different times were superposed incoherently and high space-frequency components were eliminated; thus, we could obtain the temperature difference free of the wavefront deformation in the optical elements and the window of the experimental cell. This technique was equivalent to measuring the displacement or the bending angle of fringes. As a reference, we used the interferogram when the cell was in the isothermal condition (upper interferogram), which was achieved in the first stage of the experiment (just before the experimental cell was cooled). The property of the moiré technique to calibrate the errors of the two-beam interferometry was similar to that in holography.

We used salol (phenyl salicylate, $C_{13}H_{10}O_3$) as a model material instead of liquid crystal material. Salol has a large heat of fusion (4.65 kcal/mol) and the liquid phase can be supercooled to more than 30 deg below the melting point (T_m = 41.5°C).[6] The solid–liquid interface shows a faceted form with a particular face, which resembles that of the liquid crystal material.[4] After the sample was repeatedly melted and solidified in a vacuum glass tube to repel solved oxygen and then purified by zone refining, it was poured into the experimental cell. Temperature distribution in the melt was calculated from the refractive index obtained by interferometry, with consideration of its temperature coefficient.[7]

The experimental cell was composed of a glass cuvette and copper blocks. Quartz glass of 2 mm thickness was fused to a glass cuvette with inner dimensions of 12 mm (height) × 15 mm (width) × 2 mm (depth). The depth was determined

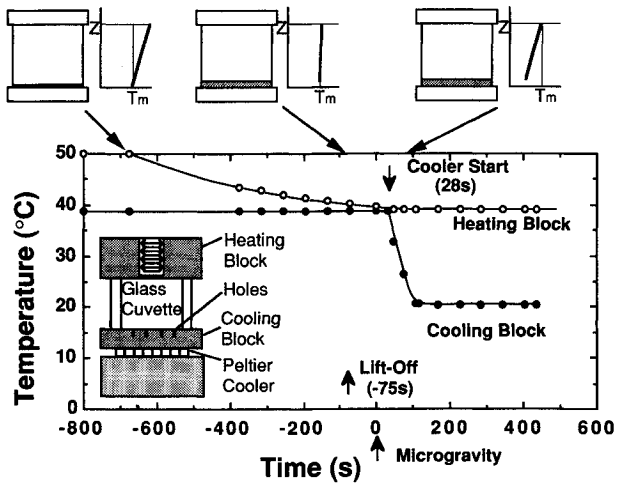

Fig. 2 Temperature profile.

because the crystal did not grow so fast in the depth direction. The glass cuvette was sandwiched by a heating and a cooling block. Temperatures of the blocks were measured using a platinum thermometer and controlled within 0.1°C of the desired temperature. Since nucleation did not occur at the cooling block at moderate temperatures, solidification should begin from a seed crystal. Holes with a diameter of 1 mm were made in the cooling block to hold the seed crystal. After pouring the sample into the cell, a solid phase was grown from the seed crystals. The holes kept the seed crystals in the cooling block and prevented them from detaching due to vibration at the launch. Although the solidification started from the seed crystals, the seed did not grow to a single crystal, but to a polycrystalline one consisting of many facets due to the large supercooling.

Figure 2 shows the temperature profile applied to both the heating and cooling blocks during the flight experiment. Fifty min before launching, the sample was melted by raising the temperature of the heating block, and then the temperature was held at 50°C. On the other hand, the temperature of the cooling block was maintained at 39°C (2.5°C below the melting point) to keep the seed crystal in the cooling block. The position of the interface was estimated to be about 2.7 mm from the cooling block. The condition of the experimental cell is also shown in Fig. 2. Since the moiré technique requires a reference interferogram, especially in the isothermal condition, the experimental cell should be set in that condition. The temperature of the heating block was reduced to 39°C, 675 s before the microgravity environment was attained, which was comparable to the characteristic time for the temperature relaxation in the cell. The crystal slowly began to grow at a rate of less than 0.005 mm/s,[6] forming a faceted face in the isothermal condition. Although changes in the gravitational field during the launch might affect the growth, the temperature gradient in the cell was so small that we hardly observed noticeable changes during the vibration test.

Observation was initiated when the microgravity condition was reached (75 s after launching). The crystals grew to 4 mm from the cooling block. Twenty-eight s after attaining microgravity, the cooling block was suddenly chilled by a Peltier cooler to 20°C, and the sample began to be unidirectionally solidified in the experimental cell. Since the temperature of the cooling block was designed to decrease more quickly than the growth rate, the temperature of the liquid was lowered below the melting point. There was a positive temperature gradient in the melt, which restricted the protrusion of solid phase into the supercooled melt and made the interface flat, because the protruded part would be closer to the hotter melt. For comparison, the same temperature profile was applied to a ground-based experiment in the same configuration; the cell

Table 1 Physical properties

Property	Value
Melting temperature	41.5°C
Density of solid	1.321 g/cm^3
Density of liquid	1.181 g/cm^3
Thermal conductivity of solid	0.251 J/m·s·K
Thermal conductivity of liquid	0.180 J/m·s·K
Thermal diffusivity of solid	1.650 × 10^{-7}m^2/s
Thermal diffusivity of liquid	0.965 × 10^{-7}m^2/s

was cooled from the bottom, which was stable against macroconvection, because the higher temperature part was found at the upper position.

Analytical

For a system with a large heat of fusion, both the kinetic process on the interface and the diffusion process of latent heat in the melt should be considered. We calculate both the behavior of the interface advancing in the z direction and the one-dimensional time-dependent diffusion field during unidirectional solidification. Table 1 shows the parameters in this analysis.[7] For simplicity, all physical properties are assumed to be constant. The effect of convection is not considered. The heat loss from the quartz glass is also ignored. Although the 012 and 112 faces of the rhombohedral crystal grow, we neglect them and the vector normal to the interface is set in the z direction.

Thermal diffusion dominates the process and the diffusion equation is described for the solid and the liquid:

$$\frac{\partial T_j}{\partial t} = \alpha_j \frac{\partial^2 T_j}{\partial z^2} \qquad (j = s, l) \tag{1}$$

Growth rate is controlled by the diffusion of latent heat from the interface. The energy conservation law across the interface is given by

$$\rho L V(t) = \lambda_s \left.\frac{\partial T_s}{\partial z}\right|_i - \lambda_l \left.\frac{\partial T_l}{\partial z}\right|_i \tag{2}$$

When a faceted crystal grows into the supercooled melt, the interface temperature is not equal to the melting temperature. In the case when kinetics controls growth, the growth rate is also a function of interface temperature. The growth rate in the isothermal condition in a thin glass cell with a thickness of 0.25 mm is used,[6] where the latent heat is easily transferred from the glass wall:

$$V(t) = f(T_i) \tag{3}$$

Such a moving boundary problem is complicated because the phase boundary moves with time, but the physical boundary does not. In this study, coordinate transformation is conducted on Eqs. (1–3) according to the method of Duda[8]:

$$\eta_s = [z/R(t)] \qquad [0 \le z \le R(t)] \tag{4}$$

$$\eta_l = \{(Z - z)/[Z - R(t)]\} \qquad [R(t) \le z \le Z] \tag{5}$$

By this procedure, the moving boundary is transformed into a fixed boundary. This method is easily extended to a two-dimensional calculation that involves the Navier–Stokes equation.[9]

After the coordinate transformation, the equations are nondimensionalized by the following variables, where ($\bar{}$) denotes nondimensional:

$$\bar{t} = (\alpha_s t/Z^2), \qquad \bar{\eta}_j = \eta_j/Z \tag{6}$$

and Eqs. (1–3) are transformed as follows:

$$\frac{\partial T_l}{\partial \bar{t}} = \frac{\alpha_l/\alpha_s}{(1 - \bar{R})^2} \frac{\partial^2 T_l}{\partial \bar{\eta}_l^2} + \frac{(1 - \bar{\eta}_l)\dot{\bar{R}}}{1 - \bar{R}} \frac{\partial T_l}{\partial \bar{\eta}_l} \tag{7}$$

$$\frac{\partial T_s}{\partial \bar{t}} = \frac{1}{\bar{R}^2} \frac{\partial^2 T_s}{\partial \bar{\eta}_s^2} + \frac{\bar{\eta}_s \dot{\bar{R}}}{\bar{R}} \frac{\partial T_s}{\partial \bar{\eta}_s} \tag{8}$$

$$\dot{\bar{R}} = \frac{C_{p_s}}{L\bar{R}} \left[\frac{\partial T_s}{\partial \bar{\eta}_s} - \frac{\lambda_l/\lambda_s}{1 - \bar{R}} \frac{\partial T_l}{\partial \bar{\eta}_l}\right]_i \tag{9}$$

$$\dot{\bar{R}} = \bar{V}(\bar{t}) = \frac{Z}{\alpha_s} f(T_i) \tag{10}$$

These equations are solved by the finite difference method. At first, the temperatures of the heating block and the cooling block are 39 and 20°C, respectively. The initial temperature distribution is assumed to be linear between the two blocks. The interface is located 4 mm from the cooling block, which is the condition about 100 s after the start of the experiment.

Results and Discussion

Figure 3 shows the interferograms obtained for both the ground-based and flight experiments. The solid phase advanced from the bottom and fringes appeared in front of the interface. The left side of each interferogram was obtained by the infinite method, where each infinite fringe corresponded to a temperature difference of 0.73°C. The right side was obtained by the finite method, which enabled us to measure the temperature of the interface and the temperature gradient around it by analyzing the bending of fringes. Fringes made by the wedge inclined to the right when the cell was cooled from the cooling block.

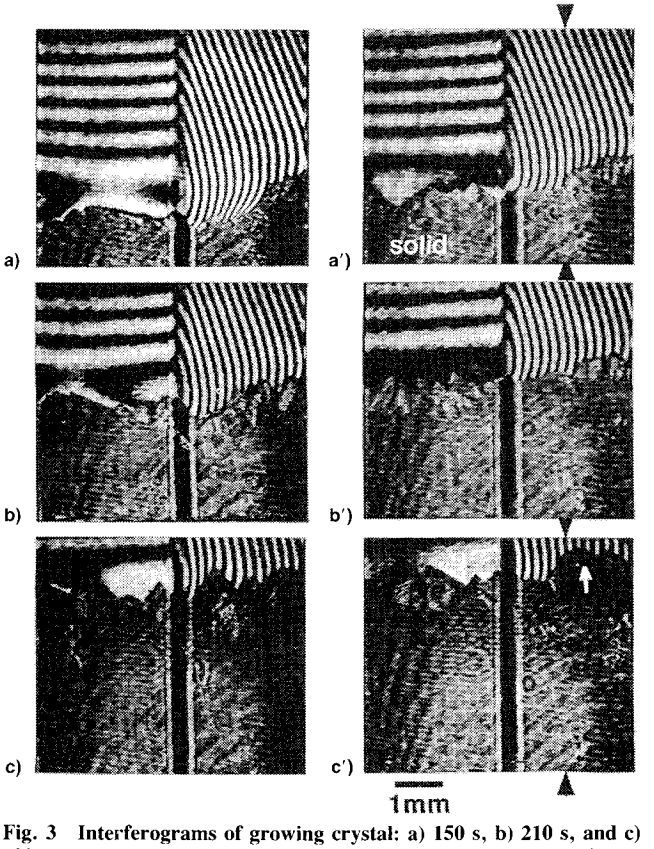

Fig. 3 Interferograms of growing crystal: a) 150 s, b) 210 s, and c) 300 s; ground-based experiment and a') 150 s, b') 210 s, and c') 300 s; flight experiment.

At 150 s, supercooling of the interface was estimated to be about 8°C by measuring the displacement of fringes. A temperature-reversed layer was observed in front of the interface, where the finite fringes changed their inclination. The effect of the crystal habit was small, as shown in Figs. 3a and 3a′. As the interface advanced, its temperature increased and each faceted crystal became larger than 1 mm, as shown in Figs. 3c and 3c′, at 300 s. The ambient temperature near the interface was about 39°C and close to the melting point where the viscosity and the growth velocity became low. In the microgravity condition, it was found that the solid phase with some facet faces advanced freely and protruded into the melt, as shown by the arrow in Fig. 3c′. The protrusion of the crystal was suppressed in the ground-based experiment due to the fluidity of the melt near the interface. However, interferometry could provide information on temperature distribution, but not on fluid motion.

Figure 4 shows the position of the interface measured from the cooling block and its standard deviation. Positions on the interface (256 points) were digitized from images, and their mean value $\bar{R}(N)$ and standard deviation $\sigma(N)$ on the scale of N were calculated:

$$\sigma^2(N) = \frac{1}{N}\sum_{i=1}^{N}[R_i - \bar{R}(N)]^2, \quad \bar{R}(N) = \sum_{i=1}^{N} R_i \quad (N \le 256) \tag{11}$$

Standard deviation represents the roughness of the interface on the scale of N, of which dependence on N shows a fractal dimension. Recently, the self-affine fractal structure has been reported, where the polycrystalline crystal of NH_4 was grown from an aqueous solution.[10] The dents on the interface were considered to be the main forces in the formation of such structure.

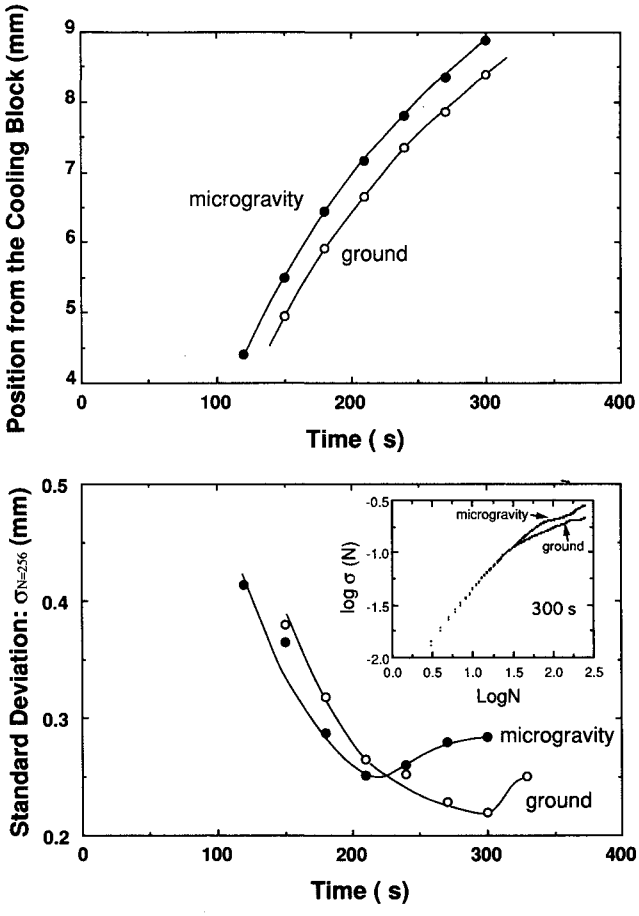

Fig. 4 Position and standard deviation of the interface (experiment).

Although the growth rate was almost the same for both ground and microgravity experiments, it was found that the standard deviation ($N = 256$) of the interface became greater after 210 s in microgravity. Before chilling of the cooling block, the standard deviation became large in the isothermal condition. The protruded part of the interface was not restricted because it was close to the more supercooled region to which a little latent heat was transferred from the interface. When the temperature gradient was applied to the interface, the growth of the protruded crystals was restricted by a higher-temperature melt existing ahead. Considering the characteristic time for thermal relaxation, the interface was gradually stabilized, which was the cause of the decrease in the standard deviation. As the crystals grew, the standard deviation became larger. One reason was related to the existence of the temperature-reversed layer, where the growth of the protruded crystals was not restricted. The standard deviation was saturated at the end of the experiment because a positive temperature gradient existed in front of the temperature-reversed layer and the standard deviation did not exceed the thickness of the temperature-reversed layer. Another reason was considered to be the change of the crystal habit, because the temperature of the interface increased with time in this configuration and each grain of polycrystalline became large. On the ground, the increase of standard deviation was significantly delayed. The difference of standard deviation was observed on a large scale (larger N). One possible cause for the difference was microconvection in the temperature-reversed layer, which was unstable to convection on the ground. However, we could not observe the phenomenon in our observation system and further study is needed.

Figure 5 shows the isotherms in the melt obtained from the right side of Fig. 3a′ using the moiré technique. In the solid phase, since almost no interferogram was obtained, the temperature distribution was not measured. For the comparison with a previously described one-dimensional calculation, the displacement of fringes was measured on the longitudinal line between the two arrows in Fig. 3a′. Figure 6a shows the one-dimensional temperature distribution in the melt obtained from the interferograms in microgravity. It was found that a temperature-reversed layer was formed in front of the solid–liquid interface. This was because the discharged latent heat raised the temperature of the interface and diffused not only to the solid, but also to the melt. At the initial stage, solidification proceeded with the higher rate and released a larger

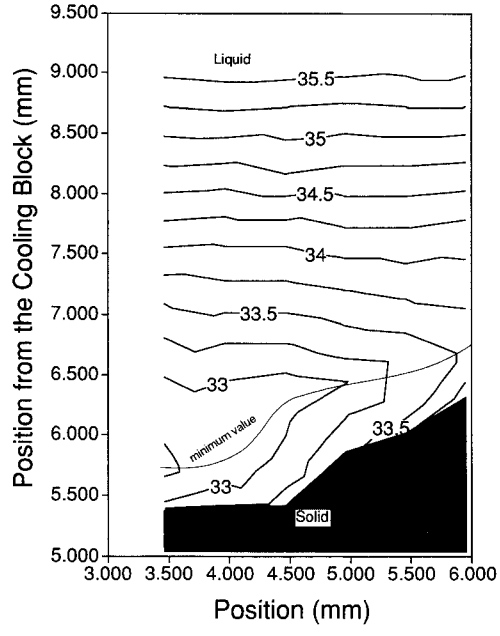

Fig. 5 Isotherms in the melt at 150 s during flight (°C).

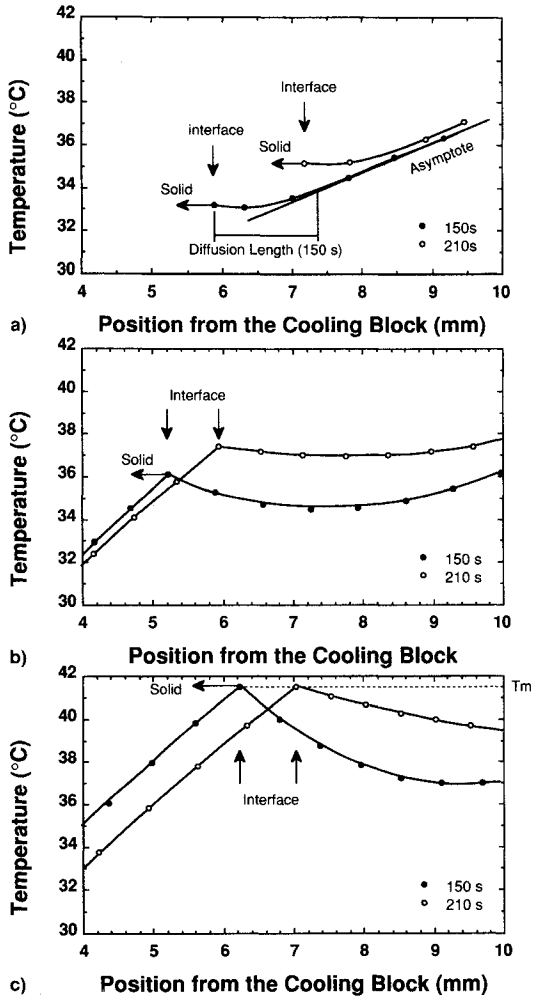

Fig. 6 One-dimensional temperature distribution in the melt: a) experimental data obtained from interferograms (flight experiment), b) analytical result in both the kinetics and diffusion controlling system, and c) analytical result in only the diffusion controlling system.

amount of heat, which caused the higher temperature increase in this layer. Since the applied temperature gradient was weakened or reversed, it could not stabilize the increase of the interface roughness; this is a reason for the protrusion of the interface. This effect was amplified as each faceted crystal grew large comparable to the thickness of the reversed layer.

Figure 6b shows the temperature distribution obtained by numerical calculation. It well explains the temperature distribution in the melt and confirms the existence of the temperature-reversed layer. As the solid advanced, the interface temperature increased. For comparison, a calculation was also carried out using the diffusion control system, where the interface temperature was set to be the melting point (Fig. 6c). Since a rate-determining step on the interface existed in the kinetics model where the growth rate was controlled by both heat transfer and kinetics on the interface, the growth rate was lower. In this condition, two-dimensional nucleation limited the kinetics, where lateral growth and crystal habit showed the nature of the crystal growth.[6]

There are differences in the values of temperature distribution, interface temperature, and growth rate between Figs. 6a and 6b. They result in the heat loss from the glass wall, which is appreciable for two reasons. The first one is that the thermal conductivity of quartz glass is five times greater than that of salol and the glass thickness (2 mm) is comparable to the sample thickness. The disagreement can be reduced by increasing the value of thermal conductivity in the calculation. Although it was desirable that the glass should be as thin as possible from the viewpoint of thermal conductivity, it had been determined by considering the distortion of the cuvette. The second cause of the disagreement was that the temperature increase was not always homogeneous through the light path and the temperature was underestimated.

The validity of the temperature measurement must be discussed next because the refractive index of the liquid itself was considerably varied depending on the concentration of impurities. We considered the diffusion length, which was defined by

$$l = 2D/V(t) \tag{12}$$

At 150 s, the diffusion length was obtained to be 1.46 mm, considering the deviation of the temperature profile from the linear asymptote, as shown in Fig. 6a, and the growth rate was measured to be 0.03 mm/s from the experimental data. From Eq. (12), the diffusion coefficient was estimated to be 0.02 mm^2/s, which was on the same order as the thermal diffusivity of liquid (α_s: 0.095 mm^2/s in Table 1). We concluded that the change of the refractive index is mainly caused by the thermal diffusion for the following reasons: the diffusion coefficient of impurities in the organic material is much smaller than these values (two orders lower) and the impurities accumulated in front of the interface infinitely. No appreciable diffusion layer was observed during the latter part of the experiment because the temperature difference was too small to be measured. For this reason, the diffusion coefficient is related to the thermal one. It should be noted that this layer appeared only when the solid grew into the supercooled melt, which was confirmed by the analysis.

Conclusions

Using interferometry, the temperature distribution in front of the interface of salol solidifying into the supercooled melt was observed. To investigate the transfer of latent heat, the finite fringe method was applied for precise measurement of the temperature distribution as well as the interface temperature. A temperature-reversed layer appeared in an applied temperature gradient. Interface protrusion into the supercooled melt under the microgravity condition showed that the applied temperature gradient was changed due to the following causes: the growth of the temperature-reversed layer and the effect of the crystal habit. Therefore, the roughness of the interface was amplified. On the other hand, the protrusion was restricted under the ground-based conditions.

The one-dimensional diffusion field was analyzed, considering the kinetics of the interface. It was found that the growth rate in the experiment was higher than the calculated one because the heat loss from the glass cell occurred in the experiment. However, the behavior of temperature distribution and the interface temperature agreed qualitatively.

Acknowledgments

This work was carried out with the aid of funds from the Mechanical Social Systems Foundation and the Society of Japanese Aerospace Companies, Inc.

References

[1]Hurle, D. T. J., Muller, G., and Nitsche, R., "Crystal Growth from the Melt," *Fluid Science and Material Science in Space*, edited by H. U. Walter, Springer–Verlag, Berlin, 1987, pp. 313–354.

[2]McCay, M. H., and McCay, T. D., "Experimental Measurement of Solutal Layers in Unidirectional Solidification," *Journal of Thermophysics and Heat Transfer*, Vol. 2, No. 3, 1988, pp. 197–202.

[3]Ecker, A., "Two-Wavelength Holographic Measurement of Temperature and Concentration During Alloy Solidification," *Journal of Thermophysics and Heat Transfer*, Vol. 2, No. 3, 1988, pp. 193–196.

[4]Iwasaki, A., Hosokawa, S., Kudo, I., Tanimoto, M., Sakurai, H., Arai, Y., Watanabe, T., Kawai, S., Ishikawa, M., and Kamei, S., "Visualization of a Solidification Process in Microgravity," *Jour-*

nal of Thermophysics and Heat Transfer, Vol. 6, No. 3, 1992, pp. 733–737.

[5]Yokozeki, S., and Mihara, S., "Moire Interferometry," *Applied Optics*, Vol. 18, No. 7, 1979, pp. 1275–1280.

[6]Jackson, K. A., Uhlmann, D. R., and Hunt, J. D., "On the Nature of Crystal Growth from the Melt," *Journal of Crystal Growth*, Vol. 1, No. 1, 1967, pp. 1–36.

[7]Durig, U., Bilgram, J. H., and Kanzig, W., "Properties of the Solid-Liquid Interface of Growing Salol Crystals," *Physical Review A*, Vol. 30, No. 2, 1984, pp. 946–959.

[8]Duda, J. L., Malone, M. F., Notter, R. H., and Vrentas, J. S., "Analysis of Two-Dimensional Diffusion-Controlled Moving Boundary Problems," *International Journal of Heat and Mass Transfer*, Vol. 18, Nos. 7/8, 1975, pp. 901–910.

[9]Saito, T., "Numerical Method for Multi-Dimensional Freezing Problem in Arbitrary Domains," *Journal of Heat Transfer*, Vol. 100, No. 2, 1978, pp. 294–299.

[10]Honjo, H., and Ohta, S., "Self-Affine Fractal Crystal from an NH_4Cl Solution," *Physical Review E*, Vol. 49, No. 3, 1994, pp. R1808–1810.